PNAS RESEARCH ARTICLE | NEUROSCIENCE OPEN ACCESS

Synaptic Gα12/13 signaling establishes hippocampal PV inhibitory circuits

Krassimira Garbett[a,1], Baris Tosun[a,1], Jaybree M. Lopez[a], Cassandra M. Smith[a], Kelly Honkanen[a], and Richard C. Sando[a,2]

Edited by Alex Kolodkin, Johns Hopkins University School of Medicine, Baltimore, MD; received April 18, 2024; accepted November 4, 2024

Combinatorial networks of cell adhesion molecules and cell surface receptors drive fundamental aspects of neural circuit establishment and function. However, the intracellular signals orchestrated by these cell surface complexes remain less understood. Here, we report that the Gα12/13 pathway lies downstream of several GPCRs with critical synaptic functions. Impairment of the Gα12/13 pathway in postnatal hippocampal neurons diminishes inhibitory inputs without altering neuronal morphology or excitatory transmission. Gα12/13 signaling in hippocampal CA1 neurons in vivo selectively regulates PV interneuron synaptic connectivity, supporting an inhibitory synapse subtype-specific function of this pathway. Our studies establish Gα12/13 as a signaling node that shapes inhibitory hippocampal circuitry.

G protein-coupled receptors | synapse | cell signaling | G protein signaling | interneurons

Neural circuits are composed of structurally and physiologically diverse synaptic connections that assemble into stereotyped circuits during development (1–3). Once organized synaptic connectivity is established, circuits are continuously modified by experience and maintained over an individual's lifetime. Despite the identification of a multitude of behaviorally relevant circuits, the cellular mechanisms underlying how these circuits are established and function remain incompletely understood (4, 5).

For several decades, extracellular molecular codes have been postulated to direct synapse formation and modulate the functional parameters of synapses, and an array of synaptic adhesion molecules and cell surface receptors have validated this hypothesis (6–8). These include synaptic adhesion molecules essential for directing the functional properties of synapses, such as presynaptic Neurexins and their postsynaptic binding partners Neuroligins, LRRTMs (Leucine rich repeat transmembrane proteins), and Calsyntenins (9). While these extracellular networks are critically important, circuit assembly and function also require signaling cascades emanating from extracellular protein complexes. The bidirectional trans-synaptic intracellular signaling pathways driving circuit establishment remain relatively understudied (10–12).

Several G protein-dependent pathways have well-documented roles in synapse assembly and function. For example, the Gαs/cAMP pathway has been shown to promote excitatory synapse formation (13–15) and has extensive roles in excitatory synaptic function and plasticity (16–18). Furthermore, the adhesion G protein-coupled receptors (aGPCRs), including LPHNs (latrophilins), BAIs (brain angiogenesis inhibitors), and CELSRs (cadherin EGF LAG seven-pass G-type receptors), function in synapse formation and circuit assembly (19–42). aGPCRs participate in extracellular adhesion complexes while also controlling intracellular G protein-mediated signal transduction, thus exemplifying synaptic adhesion molecules with dual adhesion and signaling functions.

While these synaptic functions have been established, how synaptic aGPCRs function as receptors to coordinate intracellular signal transduction in neural circuits remains incompletely understood (43, 44). The prevailing models for aGPCR activation center around the tethered agonist peptide (TA or Stachel peptide), a membrane proximal sequence in the aGPCR signature GAIN (GPCR autoproteolysis inducing) domain (45–47). However, studies which examined all 33 human aGPCRs found only a subset likely utilize a TA-dependent mechanism (48), consistent with several modes of aGPCR activation (49–51). Moreover, these studies found a notable preference of aGPCRs for Gα12/13 (48), and several synaptic aGPCRs have been shown to activate Gα12/13 including LPHN2 and LPHN3 (52). Despite these observations, the roles of Gα12/13 signaling at synapses are not well-defined.

Here, we investigate the signaling pathways directing synaptic function and neural circuit assembly in mammalian hippocampal neurons. Building on previous work outlined above, we find that the Gα12/13 pathway is activated by several GPCRs with critical importance at synapses. Therefore, we tested the function of Gα12/13 in mature hippocampal synapses.

Significance

The mammalian brain is composed of a remarkable number of physiologically diverse synaptic connections that assemble into neural circuits during development. Information processing by this circuitry guides behavior. Extracellular adhesion complexes and cell surface receptors drive central aspects of circuit establishment and synaptic function. However, the intracellular signals coordinated by these molecular networks remain less understood. Our results show that several synaptic receptors promote Gα12/13 activation and that this G protein pathway has a critical function at inhibitory synaptic connections in hippocampal circuits. These studies help illuminate the intracellular signaling processes that shape mammalian neural circuits.

Author affiliations: [a]Department of Pharmacology, Vanderbilt Brain Institute, Vanderbilt University, Nashville, TN 37240

Author contributions: K.G., B.T., and R.C.S. designed research; K.G., B.T., J.M.L., C.M.S., K.H., and R.C.S. performed research; K.G., B.T., J.M.L., C.M.S., K.H., and R.C.S. analyzed data; and K.G., B.T., J.M.L., C.M.S., K.H., and R.C.S. wrote the paper.

The authors declare no competing interest.

This article is a PNAS Direct Submission.

[1]K.G. and B.T. contributed equally to this work.

[2]To whom correspondence may be addressed. Email: richard.sando@vanderbilt.edu.

This article contains supporting information online at https://www.pnas.org/lookup/suppl/doi:10.1073/pnas.2407828121/-/DCSupplemental.

Published December 18, 2024.

Our results show that Gα12/13 signaling is important for inhibitory synapses in a subtype-selective manner, supporting that this pathway is a component of the synapse-specific signaling networks that establish neural circuits.

Results

Several Synaptic GPCRs Activate Gα12/Gα13. Recent studies have shown that LPHNs can engage several downstream G proteins, including Gα12/13 (48, 4952). Furthermore, analysis of all 33 human aGPCRs found a notable preference for aGPCRs to activate Gα12/13 (48). To further examine the relationship between Gα12/13 and GPCRs with synaptic functions, we employed an optimized panel of BRET2 sensors termed "TRUPATH" (53) and tested several receptors, including LPHN1-3, BAI1-3, $GABA_B$, mGluR1, and β_2-adrenergic receptor (Fig. 1 and *SI Appendix*, Figs. S1–S3). For the aGPCRs, we used an approach that allows acute, inducible exposure of the native TA (Fig. 1 and *SI Appendix*, Fig. S1) (49, 52, 54, 55). We replaced the N-terminal adhesion fragment upstream of the native TA region of LPHN1-3 and BAI1-3 with HALO-FLAG (Fig. 1*A*). This approach allows for enterokinase (EK)-mediated cleavage within the FLAG sequence to acutely expose the native TA peptide (54). Therefore, this enables analysis of TA exposure-independent G protein coupling in the absence of EK, together with TA-exposure-dependent coupling after EK treatment. We first confirmed the surface expression of these six fusion constructs via HALO tag labeling, supporting their efficient expression and surface trafficking in HEK293T cells (Fig. 1*B* and *SI Appendix*, Fig. S1).

We subsequently combined this approach with a panel of TRUPATH biosensors for different Gαβγ combinations (Fig. 1 *C*–*N* and *SI Appendix*, Figs. S2 and S3). We measured basal G protein activation in the absence of EK treatment, as well as TA exposure-dependent activation after EK treatment. Of the six aGPCRs tested, LPHN2 and LPHN3 displayed evidence for TA exposure-dependent Gα12/13 activation, as shown previously (48, 52) (Fig. 1 *F*–*H* and *L*–*N* and *SI Appendix*, Figs. S2 and S3). These results also align with recent studies suggesting that LPHN1 and BAI1-3 likely lack TA-dependent signaling (48). We next tested additional GPCRs with important synaptic functions, including $GABA_B$, mGluR1, and the β_2-adrenergic receptor (Fig. 1 *O*–*R* and *SI Appendix*, Figs. S2 and S3). Again, acute LPHN2 TA-exposure activated Gα12/13 (Fig. 1*O*). Interestingly, while $GABA_B$ treated with SKF-97541 robustly activated GαoA, it also modestly activated Gα13 (56) (Fig. 1*P*). mGluR1 displayed robust activation of GαoA and Gαq, as well as Gα12 (Fig. 1*Q*). GαoA and predominately GαsS were activated via the β_2-adrenergic receptor, with no evidence of Gα12/13 activation (Fig. 1*R*). Thus, several GPCRs important for synapse formation and function can engage Gα12/13. These results also align with recent studies showing that only a subset of aGPCRs show TA-dependent signaling (48). However, the function of the Gα12/13 pathway at synapses is not well established.

Gα13 Localizes to Hippocampal Synapses and Is Essential for Inhibitory Synaptic Function. These results suggest that Gα12/13 signaling may have previously uncharacterized importance at synapses. To examine this further, we visualized the subcellular distribution of Gα13 in primary hippocampal neurons relative to LPHN1-3 and pre- and postsynaptic markers (Fig. 2 *A*–*H* and *SI Appendix*, Fig. S4 *A* and *B*). We generated primary hippocampal cultures from mouse lines containing epitope tags introduced into endogenous LPHNs; namely, Myc-LPHN1, LPHN2-mVenus, and HA-LPHN3 (Fig. 2 *A*–*D*) (19, 25, 57). Interestingly, Gα13 exhibited punctate localization that partially overlapped with LPHNs (Fig. 2 *A*–*D* and *SI Appendix*, Fig. S4*A*). Moreover, Gα13 partially colocalized with presynaptic Syn1/2, inhibitory presynaptic vGAT, and excitatory postsynaptic SHANK2 or Homer1 markers (Fig. 2 *E*–*H* and *SI Appendix*, Fig. S4*B*). We were unable to identify a reliable Gα12 antibody for similar analysis with this G protein. The lack of complete colocalization of Gα13 with any individual LPHN or synaptic marker suggests that Gα13 is present in several hippocampal synapse subtypes. Collectively, these results support that Gα12/13 signaling is downstream several GPCRs crucial for synapse assembly and function and that Gα13 localizes to hippocampal synapses.

While Gα12/13 signaling has been studied in cell migration and neurite extension during embryonic brain development (58–63), the role of Gα12/13 at synapses in the postnatal brain has not been extensively explored. Next, we generated a molecular toolbox to assess the synaptic functions of Gα12/13 (Fig. 2 *I*–*O* and *SI Appendix*, Fig. S4 *C*–*I*). We cloned Gα12/Gα13 knockdown (KD) shRNAs, scramble shRNAs, and Gα12/Gα13 KD with rescue controls and tested their efficacy via RT-qPCR, immunoblotting, and immunocytochemistry in hippocampal neurons (Fig. 2*I* and *SI Appendix*, Fig. S4 *C*–*G* and Table S1). shRNAs were driven by the H1 promoter in a dual promoter lentiviral vector that also encoded Synapsin (Syn)-driven mClover3 as a reporter. Given the known potential for shRNA off-target effects, we also generated rescue versions that coexpressed the shRNA KD together with Syn-driven, shRNA-resistant Gα12 or Gα13 followed by IRES2-mClover3. The Gα12/13 shRNA KDs virtually abolished their respective mRNA transcripts when expressed in primary hippocampal cultures (*SI Appendix*, Fig. S4*C*). Moreover, delivery of KD lentiviruses into hippocampal neurons diminished Gα13 signal via immunoblotting and immunocytochemistry, respectively (Fig. 2*I* and *SI Appendix*, Fig. S4 *D*–*G*). Coexpression of the rescue cassette restored Gα13 levels; albeit at higher levels than endogenous, as can be expected from overexpression systems (*SI Appendix*, Fig. S4 *D*–*G*). Altogether, these virally delivered reagents enable assessment of the functional role of Gα12/13 signaling in synapse assembly and physiology.

To begin determining this function, we first monitored spontaneous miniature excitatory or inhibitory postsynaptic currents (mEPSCs or mIPSCs) from double Gα12/13 KD and respective scramble control conditions (Fig. 2 *J*–*O* and *SI Appendix*, Fig. S4 *H* and *I*). Gα12/13 KD strongly diminished mIPSC frequency (Fig. 2 *J*–*L*). Conversely, mEPSC frequency and amplitude were not significantly altered (Fig. 2 *M*–*O*). None of these experimental manipulations altered the intrinsic electrical properties of recorded neurons (*SI Appendix*, Fig. S4 *H* and *I*). These results indicate an essential function of Gα12/13 at inhibitory hippocampal synapses.

We next analyzed spontaneous synaptic transmission in single Gα12 or Gα13 KD conditions to dissect their specific contribution at inhibitory synapses (Fig. 3 and *SI Appendix*, Fig. S5). Gα12 depletion alone resulted in no significant impairment in mEPSCs or mIPSCs (Fig. 3 *A*–*F* and *SI Appendix*, Fig. S5 *A* and *B*). Diminishing Gα13 alone reduced mIPSC frequency and resulted in a shift of mIPSC population amplitudes toward lower magnitudes, while again mEPSCs were unaffected (Fig. 3 *G*–*L* and *SI Appendix*, Fig. S5 *C* and *D*). These results support that the role of this pathway at inhibitory synapses is primarily driven by Gα13. However, given we cannot exclude a partial contribution or redundancy of Gα12 in this pathway, we subsequently predominately analyzed Gα12/13 KD conditions.

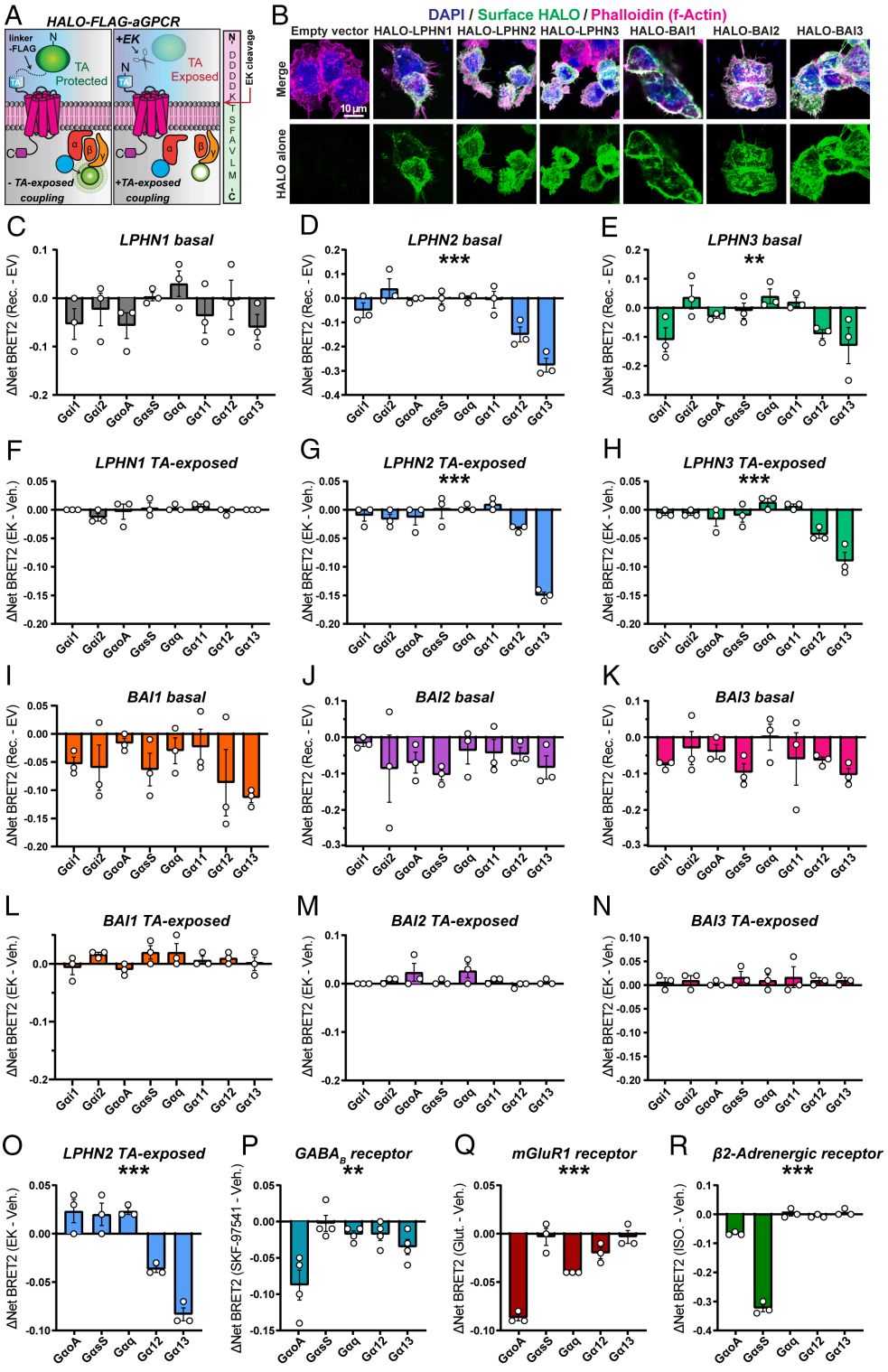

Fig. 1. Several synaptic GPCRs activate Gα12/13. (*A*) model of experimental approach. *Right*, an example FLAG-TA cleavage site using LPHN3. EK cleaves FLAG (pink sequence) following lysine, exposing the native TA (green sequence). (*B*) surface expression and localization of HALO-tagged aGPCR constructs in HEK293T cells. *Top*, merged channels; *bottom*, isolated surface HALO dye channel. (*C–E*) basal G protein coupling of HALO-FLAG fusions of LPHN1 (*C*), LPHN2 (*D*), LPHN3 (*E*) using the indicated set of TRUPATH BRET2 biosensors. For basal measurements, net TRUPATH signal from cells transfected with overexpressed constructs were compared to cells transfected with empty vector which were cotransfected with the same TRUPATH biosensors. (*F–H*) TA-exposure-dependent G protein coupling of LPHN1 (*F*), LPHN2 (*G*), LPHN3 (*H*). For exposed TA-dependent measurements, GKO HEK293 cells were transfected with the indicated TRUPATH sensor and the net BRET2 signal of cells receiving 5.5 U/well enterokinase (EK) for 15 min was compared to vehicle. (*I–K*) similar to *C–E* except for basal G protein activation of BAI1 (*I*), BAI2 (*J*), or BAI3 (*K*) fusions. *L–N*, similar to *F–H* except for TA exposure–dependent G protein activation of BAI1 (*L*), BAI2 (*M*), or BAI3 (*N*). (*O–R*) TRUPATH assays with indicated receptors. (*O*) LPHN2 TA exposure–dependent TRUPATH measurements with indicated TRUPATH biosensors. (*P*) TRUPATH assays with the GABA$_B$ receptor treated with 100 μM SKF-97541. (*Q*) similar to *O* and *P*, except for the mGluR1 receptor treated with 100 μM glutamate. (*R*) similar to *O–Q*, except for the β_2-adrenergic receptor treated with 1 μM isoproterenol. Numerical data are means ± SEM from 3 to 4 independent biological replicates (depicted as open circles). Statistical significance was assessed with one-way ANOVA (***$P < 0.001$; **$P < 0.01$). *SI Appendix*, Fig. S1 for additional data on HALO-FLAG-aGPCR characterization and *SI Appendix*, Figs. S2 and S3 for additional TRUPATH BRET2 data.

Next, we conducted evoked inhibitory and excitatory postsynaptic current (eIPSC or eEPSC) measurements to further evaluate the functional consequences of Gα12/13 depletion on synaptic function (Fig. 4 and *SI Appendix*, Fig. S6). Gα12/13 KD substantially diminished eIPSC peak amplitude, supporting reduced inhibitory synaptic drive (Fig. 4 *A* and *B*). eEPSC amplitudes were unaffected (Fig. 4 *C* and *D*). Importantly, eIPSC and eEPSC paired-pulse ratios were also not significantly altered, suggesting no changes in presynaptic release probability (Fig. 4 *E–H*). Together with our analysis of spontaneous transmission, these results support a role of Gα12/Gα13 at inhibitory hippocampal synapses.

To further examine the specificity of our results, we conducted mIPSC rescue experiments using the lentiviral transduction paradigm (Fig. 5 and *SI Appendix*, Fig. S7). Importantly, mIPSC reductions in KD conditions were restored with the rescue approach (Fig. 5 *A–D* and *SI Appendix*, Fig. S7*A*). These results support the specificity of our shRNA effects for Gα12/13 depletion. We next performed mIPSC recordings with a sparse transfection paradigm (Fig. 5 *E–H* and *SI Appendix*, Fig. S7*B*). While

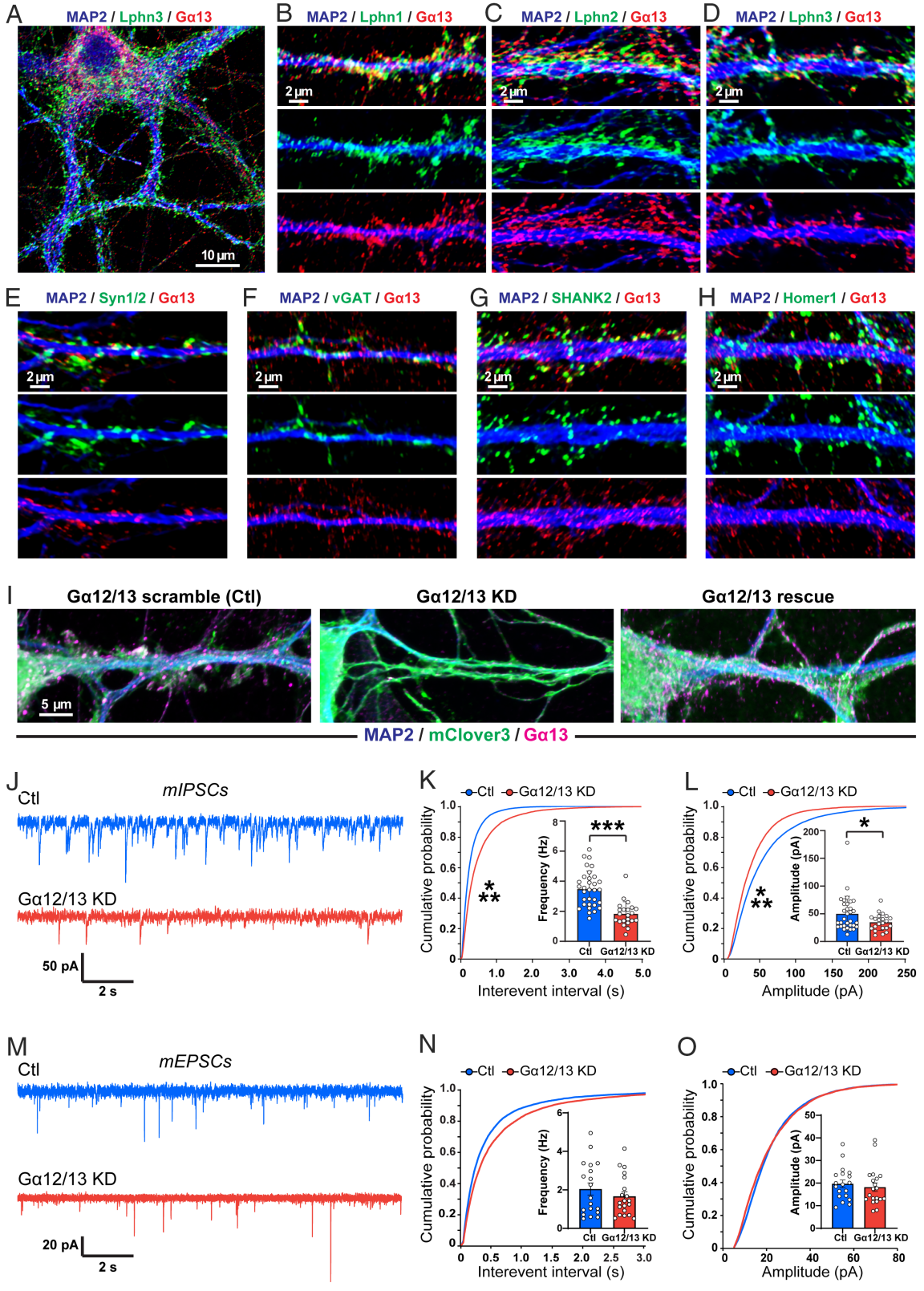

Fig. 2. The Gα12/13 pathway is essential for inhibitory synaptic function in hippocampal neurons. (*A*) representative primary hippocampal neuron immunolabeled for Gα13 together with HA-tagged endogenous LPHN3 and the somatodendritic marker MAP2. (*B-D*), colocalization of Gα13 with LPHN1-3 in primary hippocampal neurons. Primary neurons from mouse lines with endogenously tagged LPHN1-3 (19, 25, 57) were colabeled with Gα13, MAP2, and Myc-LPHN1 (*B*), LPHN2-mVenus (*C*), or HA-LPHN3 (*D*). (*E–H*) primary neurons colabeled for Gα13 and Syn1/2 (*E*), vGAT (*F*), SHANK2 (*G*), or Homer1 (*H*). MAP2 was used as a somatodendritic marker. (*I*) validation of Gα12/13 KD and rescue system. Primary hippocampal neurons were infected with lentiviruses encoding indicated conditions together with mClover3 as a reporter and immunolabeled for Gα13 and MAP2. (*J–L*) mIPSC recordings from primary hippocampal neurons infected with lentiviruses expressing either Gα12/13 shRNA scramble (Ctl) or Gα12/13 shRNA (KD), together with mClover3. (*J*) representative mIPSC traces. (*K*) cumulative probability plot of interevent intervals and summary graph of the mean mIPSC frequency [*Inset*]. (*L*) cumulative probability plot and summary graph [*Inset*] of mIPSC amplitude measurements. (*M–O*), similar to (*J–L*), except for mEPSC measurements. Numerical data are cumulative histograms or means ± SEM. Statistical significance was determined via Kolmogorov–Smirnov test for cumulative histograms or two-tailed *t* test for summary graphs using the number of neurons as "n" values (***$P < 0.001$; *$P < 0.05$). *SI Appendix*, Fig. S4 for colocalization measurements, additional validation of shRNA constructs, and additional electrophysiological parameters.

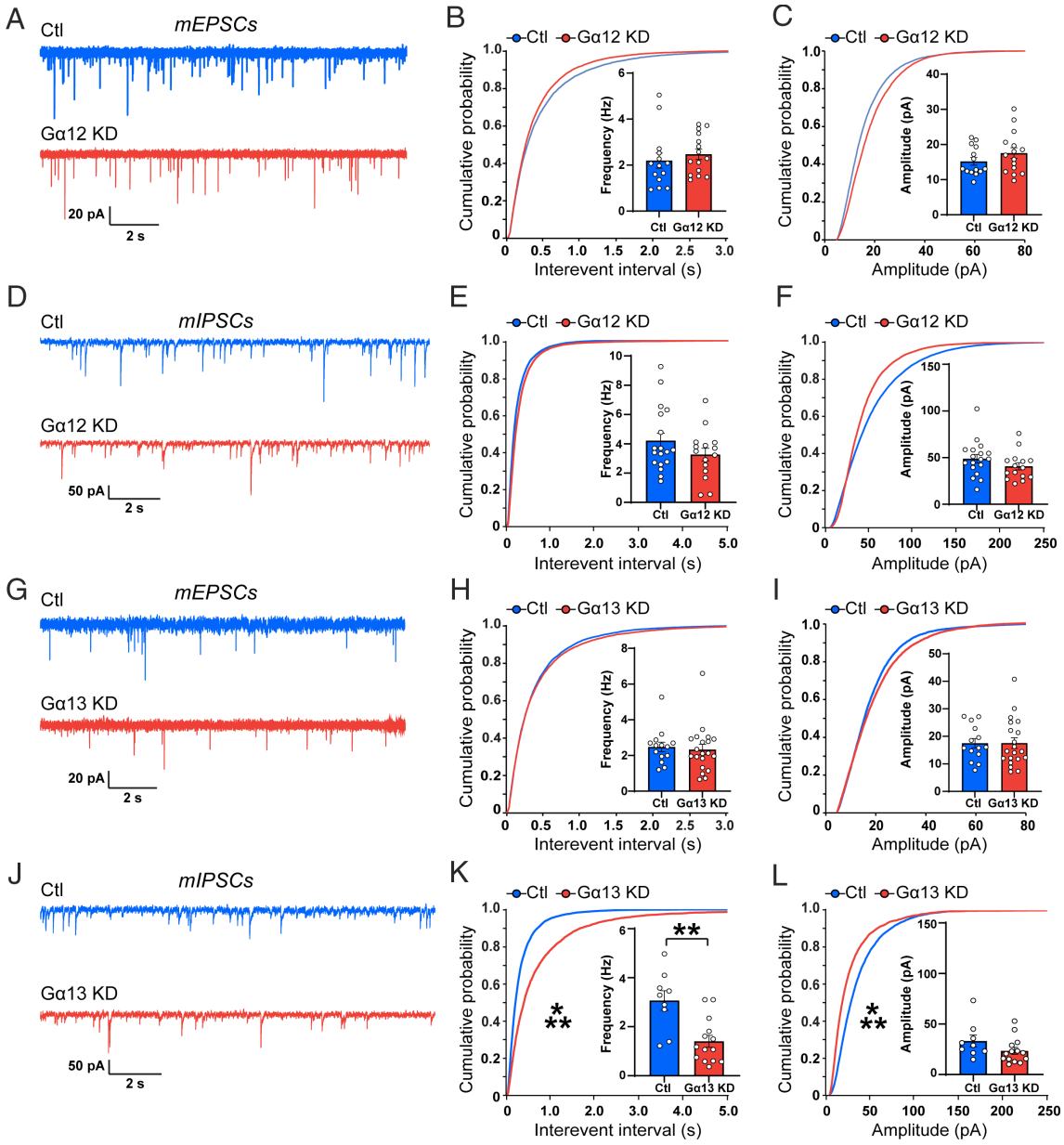

Fig. 3. Gα13 predominantly drives the role of the Gα12/13 pathway at inhibitory synapses. (*A–C*) mEPSC recordings from Gα12 control (shRNA scramble) or Gα12 KD (shRNA) conditions. Representative mEPSC traces (*A*), cumulative histograms of interevent interval and summary frequency graphs (*B*), and cumulative histograms and summary graphs of amplitudes (*C*) are shown. (*D–F*) similar to *A–C*, except mIPSC measurements from control or Gα12 KD conditions. (*G–I*) mEPSC measurements from Gα13 control (shRNA scramble) or Gα13 KD conditions. (*J–L*) similar to *G–I*, except mIPSC recordings from control or Gα13 KD conditions. Numerical data are cumulative histograms or means ± SEM. Statistical significance was determined via the Kolmogorov–Smirnov test for cumulative histograms or two-tailed *t* test for summary graphs using the number of individual recordings as "n" values (***$P < 0.001$; **$P < 0.01$). *SI Appendix*, Fig. S5 for additional electrophysiological parameters.

lentiviral transduction obtains nearly complete delivery of an experimental manipulation into primary cultures (Fig. 5*A*), the sparse transfection approach assesses cell autonomous functions with sparse delivery (Fig. 5*E*). Interestingly, cell autonomous Gα12/13 depletion resulted in no significant impairments in mIPSC frequency or amplitude (Fig. 5 *E–H*, *SI Appendix*, Fig. S7*B*). These results combined with our lentiviral studies support that the Gα12/13 pathway functions in a noncell autonomous manner to regulate inhibitory synaptic inputs.

The Gα12/13 pathway has been linked to RhoA which can induce downstream cytoskeletal rearrangement (58). To examine potential morphological impairments following Gα12/13 depletion, we conducted immunolabeling for excitatory and inhibitory synapses in Gα12/13 KD, rescue, and control conditions (Fig. 6 *A–D*). Gα12/13 depletion produced a reduction in inhibitory vGAT/Gephyrin coclusters which was restored in rescue conditions (Fig. 6 *A* and *B*). The excitatory markers SHANK2 and Homer1 were not significantly impacted upon Gα12/13 KD (Fig. 6 *C* and *D*). In parallel, we filled neurons with biocytin during electrophysiological recordings and measured dendritic branch length and dendritic spine density (Fig. 6 *E–J* and *SI Appendix*, Fig. S8). Importantly, Gα12, Gα13, or Gα12/13 KD preserved normal dendritic spine densities, primary/secondary branch numbers, and total dendritic length (Fig. 6 *E–J* and *SI Appendix*, Fig. S8). Next, we utilized sparse transfection to sparsely label neurons and measured their neurite complexity via Sholl analysis (Fig. 6 *K* and *L*). Again, we detected no substantial alterations in overall neuronal morphology using this approach (Fig. 6 *K* and *L*). These results support specific impairments at inhibitory synapses rather than general alterations in neuronal

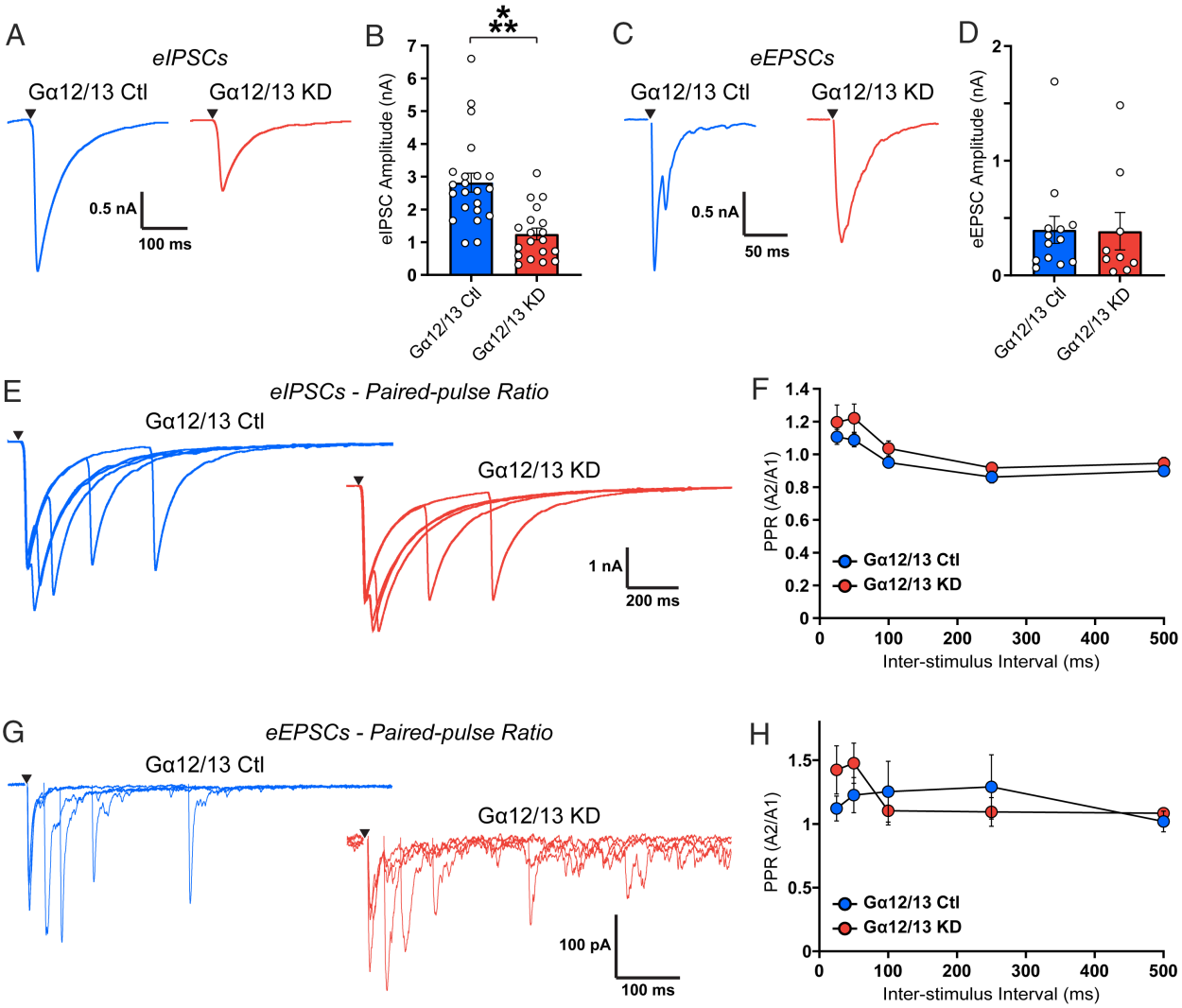

Fig. 4. Gα12/13 regulates inhibitory synaptic strength without altering release probability or evoked excitatory transmission. (*A* and *B*) evoked IPSC (eIPSC) recordings from Gα12/13 control or Gα12/13 KD conditions. (*A*) representative eIPSC traces. (*B*) summary graph of average eIPSC amplitudes. (*C* and *D*) representative evoked EPSC (eEPSC) traces (*C*) and summary graphs (*D*) from Gα12/13 control or Gα12/13 KD conditions. (*E* and *F*) eIPSC paired-pulse ratio (PPR) representative traces (*E*) and summary graphs (*F*) from control or Gα12/13 KD conditions. (*G* and *H*) similar to E and F, except for eEPSC PPR measurements. Representative eEPSC PPR traces (*G*) and summary graph (*H*). Numerical data are means ± SEM. Statistical significance was determined via two-tailed *t* test or two-way ANOVA (***$P < 0.001$). *SI Appendix*, Fig. S6 for additional electrophysiological parameters.

morphology. This helps underpin that the Gα12/13 pathway is essential for inhibitory synapse function.

Gα12/13 Selectively Regulates PV Inputs in the Hippocampal CA1 Region. We then investigated the role of the Gα12/13 pathway in hippocampal circuits in vivo. We began by injecting concentrated Gα12/13 KD and control lentiviruses bilaterally into the hippocampal CA1 region at postnatal day 0 to 1 and performed mIPSC recordings from infected CA1 pyramidal neurons 3 wk post-injection (Fig. 7 *A–D* and *SI Appendix*, Fig. S9*A*). Gα12/13 depletion in the CA1 region resulted in a significant reduction in mIPSC frequency (Fig. 7 *A–D* and *SI Appendix*, Fig. S9*A*). Moreover, the shift in mIPSC population frequency suggests a subset of inhibitory synapses in the CA1 may be affected. We then performed labeling for excitatory or inhibitory synapses throughout different subregions of the CA1 (Fig. 7 *E* and *F* and *SI Appendix*, Fig. S9 *B–H*). Gα12/13 KD reduced coclusters of inhibitory vGAT/Gephyrin throughout the CA1 region (Fig. 7 *E* and *F* and *SI Appendix*, Fig. S9*B*), yet resulted in no observable changes in excitatory vGLUT1/Homer1 coclusters or SHANK2 (*SI Appendix*, Fig. S9 *C–H*). In parallel, we filled infected CA1 neurons with biocytin during recordings and performed 3D reconstructions of dendritic arborization (Fig. 7 *G* and *H* and *SI Appendix*, Fig. S9 *I–K*). CA1 neuron dendrite arbor length and complexity were indistinguishable between Gα12/13 KD and control conditions (Fig. 7 *G* and *H* and *SI Appendix*, Fig. S9 *I–K*). We subsequently quantified their spine densities in the stratum oriens, radiatum, and lacunosum-moleculare regions and found no significant differences (Fig. 7 *I–K*), consistent with our observations in cultured neurons.

CA1 pyramidal neurons receive diverse and highly organized inhibitory inputs from an array of specific GABAergic neuronal subpopulations. To investigate the role of Gα12/13 signaling at inhibitory synapses further, we used genetically encoded reporters to label inhibitory synapses specifically from defined interneuron subpopulations in the CA1 region (Fig. 8 and *SI Appendix*, Figs. S10 and S11). We conducted concentrated lentiviral injections and coinjected an AAV encoding Cre-inducible HALO-Syb2 into mice containing the PV-Cre and Ai14 Cre reporter alleles (Fig. 8 *A–C* and *SI Appendix*, Fig. S11 *A* and *B*). This approach installed the presynaptic label HALO-Syb2 specifically into PV

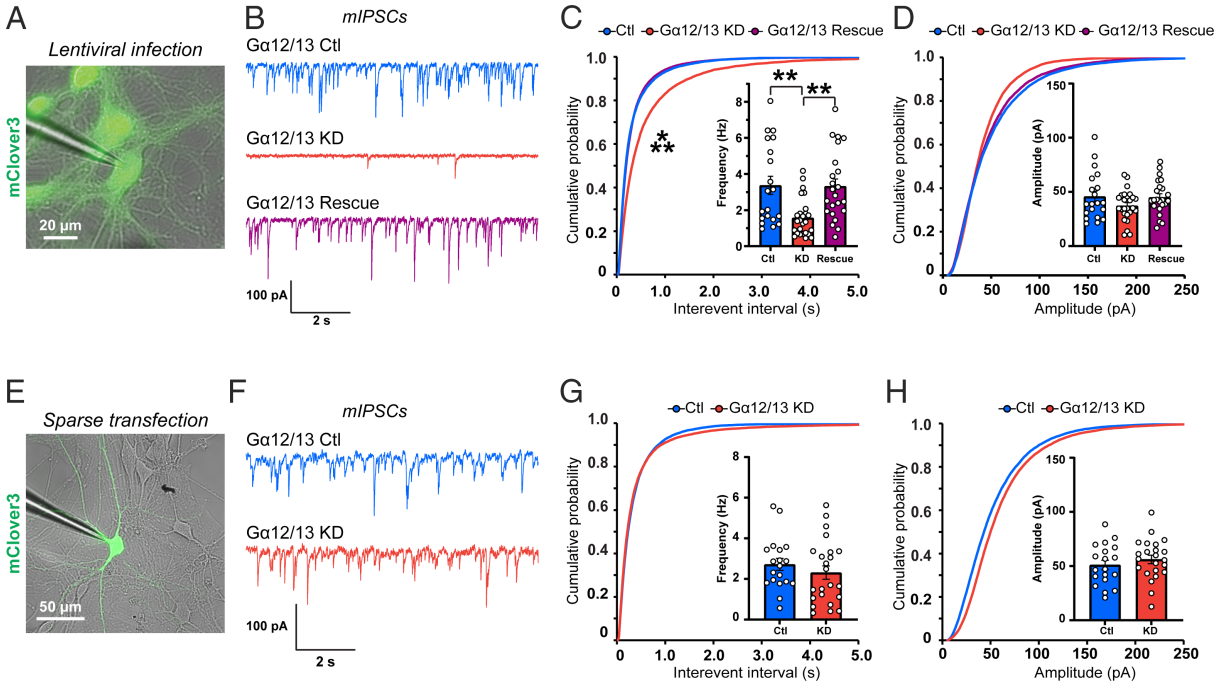

Fig. 5. Gα12/13 signaling functions in a nonautonomous manner at inhibitory synapses. (*A*) representative patched neuron from lentiviral transduction experiments in *B–D*. (*B–D*) lentiviral rescue experiments. Rescue conditions coexpressed Gα12/13 shRNAs together with shRNA-resistant Gα12 or Gα13-IRES2-mClover3. (*B*) representative mIPSC traces. (*C*) cumulative probability plot of interevent intervals and summary graph of the mean mIPSC frequency [*Inset*]. (*D*) cumulative probability plot and summary graph [*Inset*] of mIPSC amplitude. (*E*) representative patched neuron from sparse transfection experiments in *F–H*. (*F–H*) mIPSC recordings from primary hippocampal neurons sparsely transfected with indicated conditions to probe cell autonomous effects. (*F*) representative mIPSC traces from sparse transfection experiments. (*G*) cumulative probability plot of interevent intervals and summary graph of the mean mIPSC frequency [*Inset*] from sparse transfection experiments. (*H*) cumulative probability plot and summary graph [*Inset*] of mIPSC amplitude measurements from sparse transfection experiments. Numerical data are cumulative histograms or means ± SEM. Statistical significance was determined via Kolmogorov–Smirnov test for cumulative data or one-way ANOVA with post hoc Tukey tests (***$P < 0.001$; **$P < 0.01$). *SI Appendix*, Fig. S7 for additional electrophysiological parameters.

interneurons and enabled visualization of PV presynaptic terminals throughout the CA1 region. To assess the specificity of this design, we first immunolabeled sections from PV-Cre/Ai14 mice for endogenous PV and found nearly complete overlap between the Ai14 reporter and PV (Fig. 8*A*). We observed robust HALO-Syb2 labeled terminals in control and rescue conditions that were diminished upon Gα12/13 KD (Fig. 8 *A–C* and *SI Appendix*, Fig. S11 *A* and *B*).

To determine the selectivity of these effects for synapses from PV interneurons, we subsequently conducted similar experiments using SST (somatostatin)-Cre or Chrna2 (nicotinic acetylcholine receptor α2 subunit)-Cre mouse lines (Fig. 8 *D–I* and *SI Appendix*, Figs. S10 and S11). SST-Cre provides genetic access to SST-positive interneurons, while Chrna2-Cre is selective for a specific subclass of SST interneuron referred to as OLM (oriens-lacunosum moleculare) interneurons (64, 65). OLM interneurons reside in the stratum oriens layer of the CA1, but project selectively to the stratum lacunosum-moleculare region. While this line has been previously used to effectively target OLM interneurons (64, 65), we first analyzed the expression profile by crossing Chrna2-Cre mice to Ai14 and conducted histology at P21 (*SI Appendix*, Fig. S10). These experiments illustrated that while the Ai14 reporter allele is activated in various subregions throughout the brain, it is restricted to OLM interneurons in the hippocampus (*SI Appendix*, Fig. S10). We next performed similar immunolabeling control experiments in SST-Cre/Ai14 and Chrna2-Cre/Ai14 mice and found the Ai14 reporter was nonoverlapping with endogenous PV in these mouse models (Fig. 8 *D* and *G*). We subsequently labeled inputs from these interneuron populations in the CA1 using a similar Cre-inducible HALO-Syb2 approach. Control mice displayed robust presynaptic terminals labeled in the stratum lacunosum-moleculare subregion of the CA1, consistent with the expression of these Cre lines (Fig. 8 *E–I* and *SI Appendix*, Fig. S11). Importantly, the density of SST interneuron terminals was unaltered with Gα12/13 depletion, suggesting that this pathway modulates PV synapses in the hippocampal CA1. While no significant alterations in SST presynaptic inputs were observed, we detected a significant decrease in total inhibitory synapses labeled with vGAT/Gephyrin in the stratum lacunosum-moleculare (Fig. 7*F*). This difference could be due to several potential scenarios, including a function of Gα12/13 at other inhibitory synaptic subtypes we did not examine. Collectively, these studies support that the Gα12/13 pathway functions as a synaptic signaling node controlling subtype-selective inhibitory synaptic circuits.

Discussion

Extracellular protein complexes instruct synapse assembly and function. Despite substantial evidence supporting this premise, the bidirectional intracellular signals involved remain relatively understudied. Here, we report that the Gα12/13 pathway lies downstream several GPCRs with synaptic relevance and that this pathway shapes inhibitory hippocampal synapses in a subtype-selective manner. Our collective results support a model where synaptic GPCRs present in subsets of interneurons, including PV-positive interneurons, control a Gα12/13 signaling pathway that establishes subtype-specific inhibitory synapse numbers in hippocampal circuits. This pathway is likely presynaptic given the noncell autonomous effects we observed on inhibitory synapses. Thus, we postulate that compartmentalized Gα12/13 signaling in PV inhibitory synapses helps direct the establishment and function of hippocampal circuits.

Our results show a critical role of the Gα12/13 pathway in inhibitory hippocampal synapses. These studies are distinct from

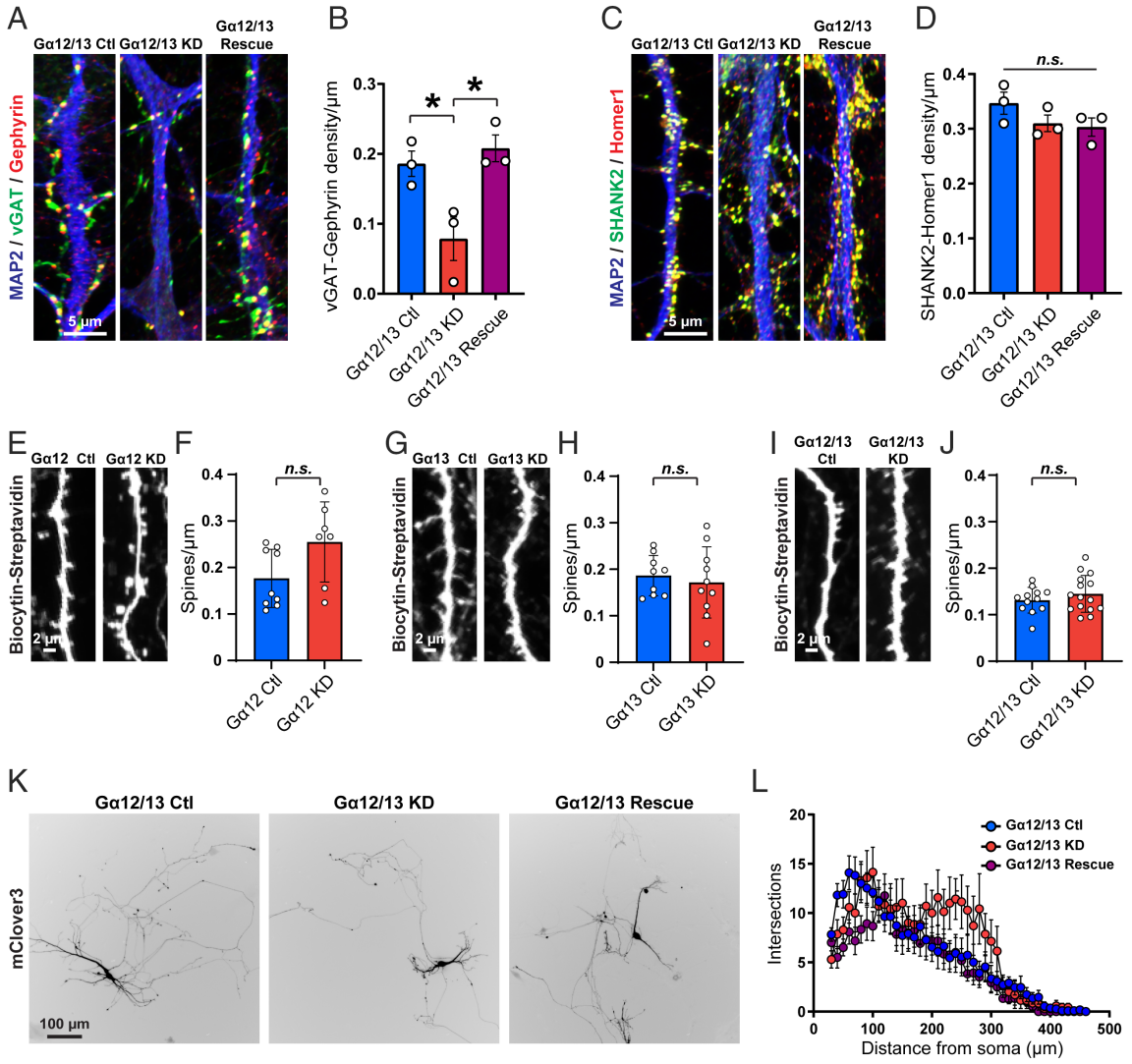

Fig. 6. Gα12/13 selectively regulates inhibitory synaptic density. (*A* and *B*) representative images (*A*) and quantifications (*B*) of neurons colabeled for vGAT, Gephyrin, and MAP2 in the indicated experimental conditions. (*C* and *D*) similar to *A* and *B*, except for neurons colabeled with SHANK2, Homer1, and MAP2. (*E* and *F*) representative spine images (*E*) and summary graphs (*F*) depicting spine density from Gα12 scramble (Ctl) or Gα12 shRNA (KD) conditions. (*G* and *H*) similar to *E* and *F*, except for Gα13 scramble (Ctl) or Gα13 shRNA (KD) conditions. (*I* and *J*) similar to *E* and *F*, except for double Gα12/13 scramble (Ctl) or Gα12/13 shRNA (KD) conditions. (*K*) representative neurons sparsely transfected with Gα12/13 control shRNAs, KD shRNAs, or rescue constructs that coexpress mClover3. (*L*) Sholl analysis of sparsely transfected neurons. Numerical data are means ± SEM from 4 to 5 independent biological replicates. Statistical significance was determined via one-way ANOVA with post hoc Tukey tests (*$P < 0.05$), two-tailed *t* test, or two-way ANOVA in Fig. 6*L*. *SI Appendix*, Fig. S8 for additional morphological parameters.

previous investigations into Gα12/13 signaling during embryonic brain development which found changes in neurite development (58–63), considering we studied Gα12/13 in postnatal neurons. Is this pathway in the postnatal brain involved directly in the initial phases of inhibitory synapse formation, or does it operate in synapse maturation or maintenance? Given the inherent challenges in definitively separating these processes, together with observations that synaptic structures are continually formed and eliminated dynamically even in mature hippocampal circuits (66), live imaging approaches monitoring synapses in Gα12/13-deficient conditions will likely be necessary toward answering this question. Given several synaptic receptors activate Gα12/13, it likely has a multifaceted role at both nascent and mature synapses.

Interestingly, while we observed Gα13 colocalization with excitatory synapses and receptors with important functions at excitatory synapses, Gα13 depletion did not alter the excitatory synaptic parameters we measured (Figs. 2–4, 6, and 7). Thus, Gα12/13 may be involved in other physiological processes at excitatory synapses, such as long-term plasticity or structural plasticity. While we report a nonautonomous effect of Gα12/13 on inhibitory synapses and partial colocalization with the inhibitory presynaptic marker vGAT (Fig. 2*F*), we did not analyze Gα13 colocalization with inhibitory postsynaptic markers. However, our results establish a foundation for additional studies directed at defining the synaptic subtype selective localization of Gα13 in neural circuits, likely by using super-resolution microscopy approaches. Moreover, the cell type-specificity of Gα12/13 function at inhibitory synapses in hippocampal CA1 circuits remains unclear. For example, Gα12/13 may be selectively expressed in PV interneurons, or may couple to specific receptors at PV interneuron synapses which are critical for synaptic function. Addressing these future questions will help define the complete Gα12/13 pathway at distinct synapses.

Consistent with previous studies (48, 52), we show that Gα12/13 can be activated by several synaptic GPCRs. However, the molecular links between specific endogenous GPCRs and Gα12/13 at inhibitory synapses remain unclear. Furthermore, regulation via non-GPCR GEFs or dedicated GAPs may

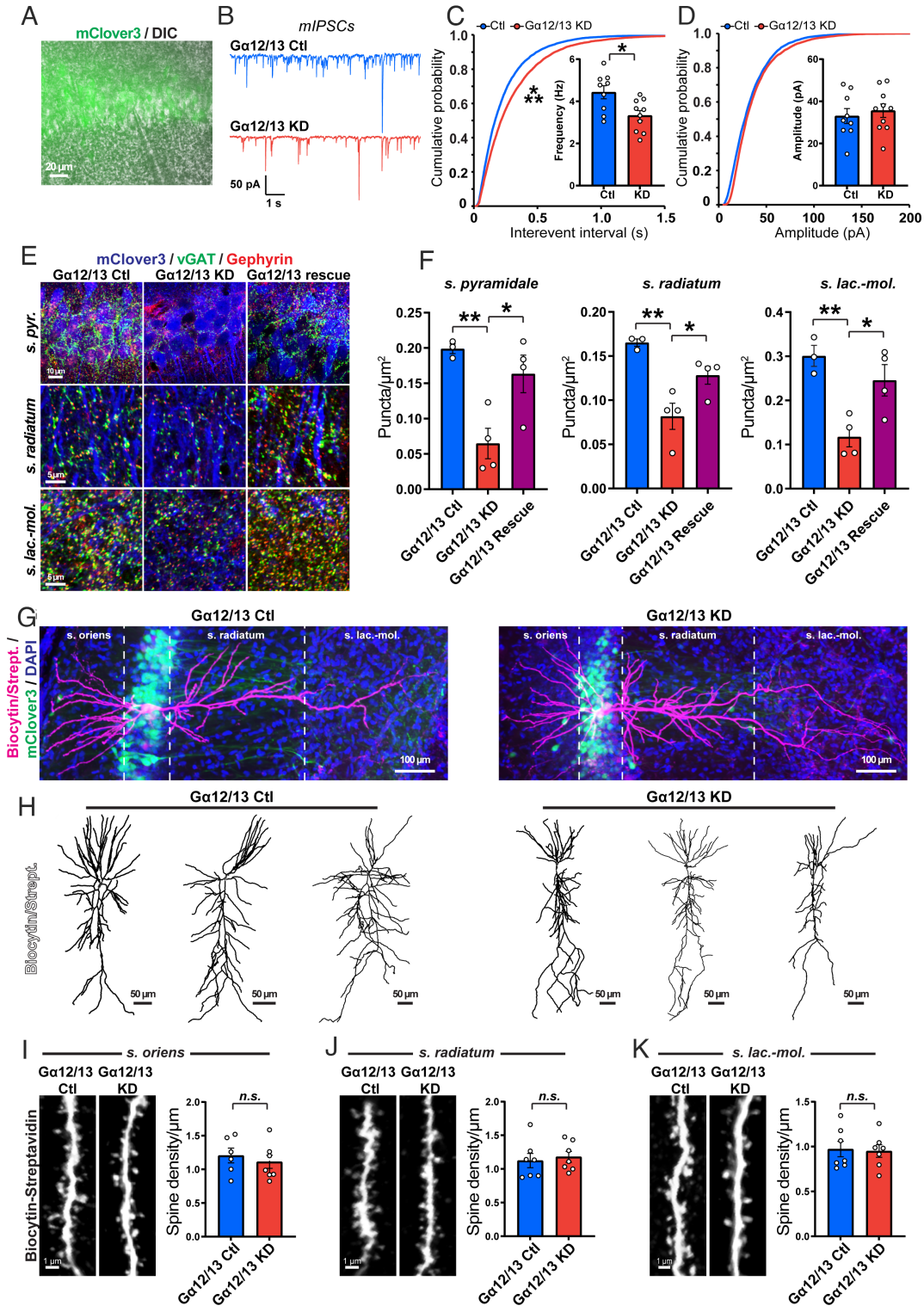

Fig. 7. Analysis of Gα12/13 function in hippocampal CA1 circuits. (*A–D*) mIPSC recordings from CA1 pyramidal neurons. (*A*) representative patched mClover3-positive CA1 neuron in acute hippocampal slices. (*B*) representative mIPSC traces from Gα12/13 scramble (control) or KD neurons. (*C*) cumulative probability plot of interevent intervals and summary graph of the mean mIPSC frequency [*Inset*]. (*D*) cumulative probability plot and summary graph [*Inset*] of mIPSC amplitude. (*E* and *F*) representative images (*E*) and quantification (*F*) of inhibitory synapses labeled with vGAT/Gephyrin in the indicated CA1 subregions from mice injected with either control, KD, or rescue viruses. (*G* and *H*) analysis of dendritic arborization from biocytin-filled CA1 neurons in panels *A–D*. (*G*) representative biocytin-streptavidin labeled neurons. (*H*) representative 3D reconstructions of biocytin labeled CA1 neurons. *SI Appendix*, Fig. S9 for quantifications. (*I–K*) quantifications of dendritic spine densities in the stratum oriens (*I*), radiatum (*J*), or lacunosum-moleculare (*K*) regions of biocytin-labeled CA1 neurons. Numerical data are cumulative histograms or means ± SEM. Statistical significance was assessed by Kolmogorov–Smirnov test, two-tailed *t* test, or one-way ANOVA with post hoc Tukey test (***$P < 0.001$, **$P < 0.01$; *$P < 0.05$). *SI Appendix*, Fig. S9 for additional imaging and electrophysiology data.

contribute to Gα12/13 synaptic function. Future studies will be necessary to unravel the receptors and Gα12/13 downstream signaling cascades controlling inhibitory circuits. RhoA is a known Gα12/13 effector, which regulates actin cytoskeletal rearrangement and the ROCK/JNK pathway. ROCK/JNK has demonstrated importance in synapse formation using heterologous synapse formation assays (15). Other effectors are likely also involved in inhibitory synapses given the physiological effects we observe together with unaltered neuronal and spine morphology.

Our studies report Gα12/13 as a signaling pathway important for hippocampal inhibitory circuitry. Insight into how the output of these signaling networks drives synapse assembly and function will inform our understanding of how neural circuits composed of a multitude of diverse synaptic connections are established in the brain.

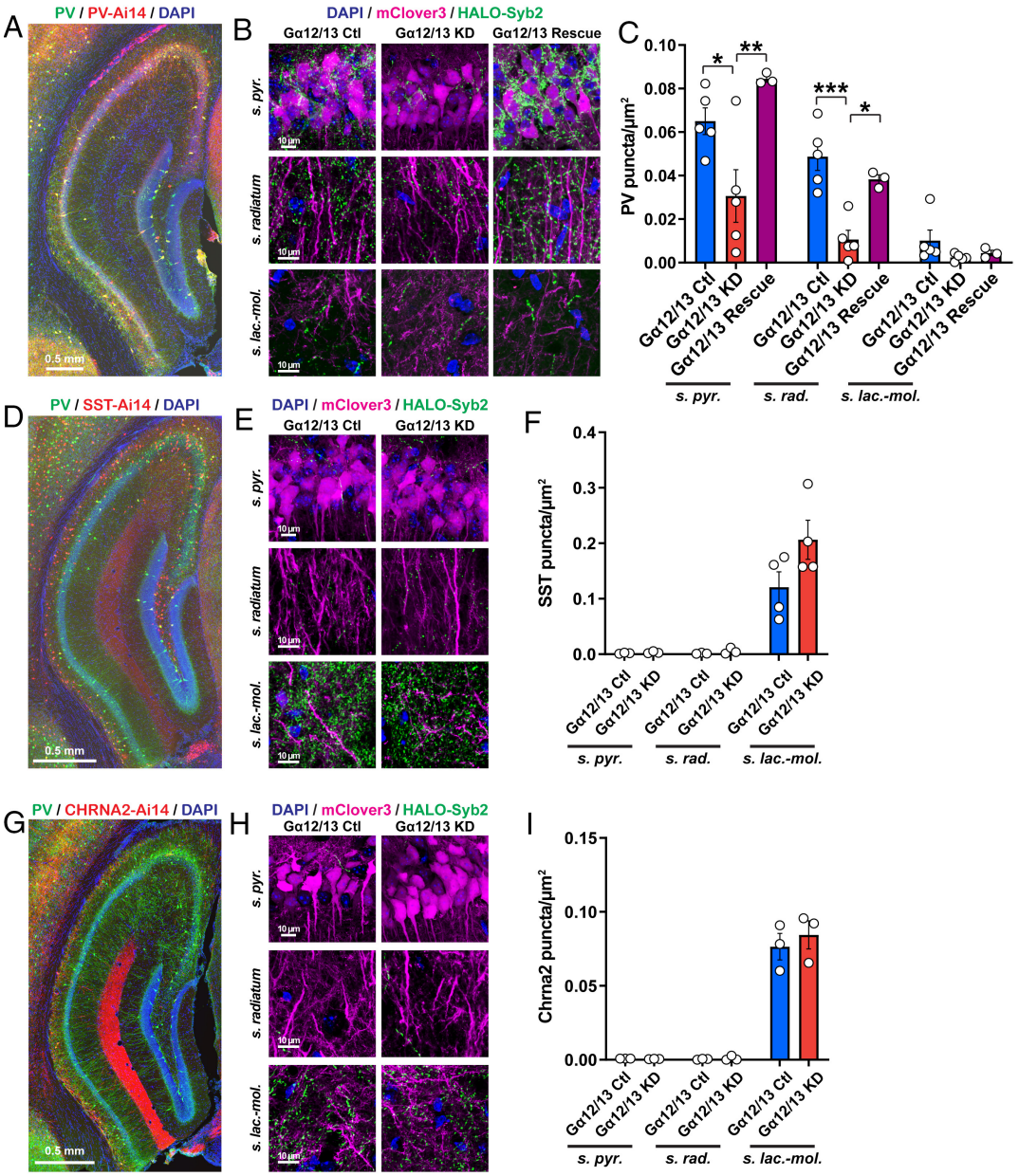

Fig. 8. The Gα12/13 pathway selectively controls parvalbumin (PV) neuron inhibitory synapses in the CA1 region. (*A–C*) concentrated lentiviruses encoding Gα12/13 shRNAs (KD), shRNA scrambles (Ctl), or rescue vectors were coinjected with AAV Syn DiO HALO-Syb2 into PV-Cre mice, enabling imaging of PV presynaptic terminals within the CA1 region. (*A*) representative image of the hippocampus of PV-Cre/Ai14 reporter mice immunolabeled for endogenous PV. (*B*) representative indicated subregions of the CA1 from PV-Cre mice injected with AAV encoding Cre-dependent HALO-Syb2 and either Ctl mClover3, KD mClover3, or Rescue mClover3 lentiviruses. (*C*) quantification of HALO-Syb2 labeled synaptic puncta density in the indicated subregions. (*D–F*) similar to *A–C*, except experiments were performed in SST-Cre mice. (*D*) SST-Cre/Ai14 sections immunolabeled for PV. (*E*) representative indicated subregions of the CA1 from SST-Cre/Ai14 mice injected with AAV encoding Cre-dependent HALO-Syb2 and either Ctl mClover3 or KD mClover3 lentiviruses. (*F*) quantification of HALO-Syb2 puncta density in indicated CA1 subregions. (*G–I*) experiments in Chrna2-Cre mice, which express Cre in OLM (oriens-lacunosum moleculare) interneurons in the CA1 region. (*G*) Chrna2-Cre/Ai14 sections immunolabeled for PV. (*H*) representative CA1 subregions from Chrna2-Cre/Ai14 mice injected with AAV encoding Cre-dependent HALO-Syb2 and either Ctl mClover3 or KD mClover3 lentiviruses. (*I*) quantification of HALO-Syb2 puncta density in indicated CA1 subregions. Numerical data are means ± SEM from 3 to 5 independent biological replicates (mice, depicted as open circles in bar graphs). Statistical significance was assessed by one-way ANOVA with post hoc Tukey test (***$P < 0.001$; **$P < 0.01$; *$P < 0.05$). *SI Appendix*, Figs. S10 and S11 for additional imaging data and further characterization of Chrna2-Cre/Ai14 mice.

Materials and Methods

Please *SI Appendix* for detailed *Materials and Methods*.

Mice. All procedures followed NIH Guidelines for the Care and Use of Laboratory Mice and were approved by the Vanderbilt University Administrative Panel on Laboratory Animal Care. The following lines were used: PV-Cre, B6.129P2-*Pvalb*$^{tm1(cre)Arbr}$/J (Jax #017320); Ai14, B6.Cg-*Gt(ROSA)26Sor*$^{tm14(CAG-tdTomato)Hze}$/J (Jax #007914), SST-Cre, *Sst*$^{tm2.1(cre)Zjh}$/J (Jax #013044); Chrna2-Cre (64, 65); Myc-Lphn1 (57); Lphn2-mVenus (19); and HA-Lphn3 (25).

Cell Lines. GKO HEK293 (67, 68) cells were maintained in DMEM (Gibco Cat# 11995065) containing 10% FBS (Gibco Cat# 16000044), 1X Penicillin-Streptomycin (Corning Cat# MT30002CI), and 1× MEM Nonessential Amino Acids (NeA) (Sigma Cat# M7145) at 37 °C/5% CO_2. HEK293T cells (ATCC #CRL-11268) were used for protein surface localization and to generate viruses. HEK293T cells were maintained in the same media above without NeA for a maximum of 25 passage numbers.

Primary Hippocampal Cultures. Bilateral hippocampi were dissected from P0 mice, dissociated by papain, filtered through a 70 μm cell strainer, and plated at 80,000 cells/mL on a PDL-coated glass coverslips in 24-well plates. Primary cells

were infected with lentiviral conditions at DIV 1, and experiments were conducted at DIV 10–14.

Plasmids. All aGPCR cDNAs were encoded in the pEB Multi-Neo vector. The HALO-FLAG-aGPCR constructs expose the native TA region after enterokinase-mediated cleavage. The TRUPATH kit was a gift from Bryan Roth (Addgene #1000000163). *Mus musculus* $GABA_B$-R1 (NM_019439.4) and $GABA_B$-R2 (NM_001081141.2) were cloned from a mouse whole brain cDNA library produced in house. pCMV5 rat mGluR1 was a gift from Dr. Colleen Niswender (Vanderbilt University). pcDNA3 Flag beta-2-adrenergic-receptor was a gift from Robert Lefkowitz (Addgene #14697). shRNA knockdown and rescue vectors were cloned in lentiviral shuttle vectors harboring both an H1 promoter and rat Synapsin promoter. For rescue vectors, silent mutations were generated in the shRNA binding site for either GNA12 (NP_034432.1) or GNA13 (NP_034433.3) to prevent shRNA binding (*SI Appendix*, Table S1). HALO-Syb2 contained HALO fused to the N terminus of rat Syb2 encoded in an EF1a promoter-driven DiO AAV2 backbone.

Antibodies. The following antibodies and reagents were used: HA rabbit (Cell Signaling Technologies, cat# 3724), GFP rabbit (Life Technologies, cat# A11122), Myc rabbit (Sigma, cat# C3956), Homer1 rabbit (Synaptic Systems, cat# 160 003), MAP2 mouse (Sigma, cat# M1406), MAP2 chicken (EnCor Biotechnology, cat# CPCA-MAP2), SHANK2 guinea pig (Synaptic Systems, cat# 162204), Syn1/2 rabbit (Synaptic Systems, cat# 106 002), VGAT guinea pig (Synaptic Systems, cat# 131004), vGLUT1 guinea pig (Millipore, cat# AB5905), Gephyrin mouse (Synaptic Systems cat# 147111), GNA13 mouse (Life Technologies, cat# 67188), β-actin mouse (Sigma, A1978), Parvalbumin rabbit (SWANT, cat # PV27a), Alexa Fluor 647 Phalloidin (Invitrogen cat# A22287), and corresponding fluorescently-conjugated goat secondary antibodies from Life Technologies. *SI Appendix* for more details including concentrations.

TRUPATH BRET2 Assays. HEK G-protein K.O. cells (67, 68) were cotransfected with the receptor of interest and TRUPATH plasmids at 1:1:1:1 DNA ratio (receptor:Gα-RLuc8:Gβ: Gγ-GFP2). For the expression of $GABA_B$ receptor, a mixture of each $GABA_B$-R1 and $GABA_B$-R2 plasmids was used. Receptors were activated by addition of (final concentrations): 0.055 U enterokinase, 100 μM L-glutamate, 100 μM SKF-97541, 1 μM isoproterenol. Luciferase luminescence was measured at 410 nm and GFP2 emission at 515 nm. The BRET ratio was calculated as GFP2 signal/luciferase signal.

RT-qPCR. Total RNA was isolated from cultured neurons at DIV10–12, and then used for cDNA synthesis with random hexamers. qPCR was used for quantification of Gα12, Gα13, and GαsS abundance, which was normalized to the expression of GAPDH.

Surface Labeling. HEK293T cells plated 1.5 to 2 × 10^5 cells/well in 0.5 mL were transfected with a receptor-expressing plasmid. Live surface labeling was accomplished 48 h posttransfection using HALO-Tag AlexaFluor488. Subsequently, fluorescently conjugated Alexa Fluor 647 Phalloidin was used for visualization of actin filaments.

Sparse Transfection. Transfections were conducted using the calcium phosphate method when primary hippocampal neurons were DIV 4 to 5. For Sholl analysis, the live cells were imaged with a Nikon Ts2-FL microscope with a 20× objective, and the analysis was performed using Nikon Elements software.

Stereotactic Injections. Injections were performed at postnatal day 21 (P21) under vaporized isoflurane anesthesia. Heads were secured to a stereotactic rig and viral solution was delivered to the CA1 bilaterally using a syringe pump to following coordinates: A/P −1.80 mm, M/L ± 1.20 mm, and D/V −1.35 mm. For neonatal injections, pups were anesthetized on ice and heads were secured to the stereotactic rig. Concentrated lentivirus solution was injected at the following coordinates: A/P −1.00 mm, M/L ± 1.00 mm and respective D/V coordinates −1.50 mm, −1.30 mm, and −1.10 mm to cover the CA1 region.

Immunohistochemistry and HALO Labeling. Perfused mouse brains were cryosectioned 25 μm thick, and the free-floating sections were labeled with primary antibodies including anti-vGAT guinea pig (Synaptic Systems #131004), anti-Gephyrin mouse (Synaptic Systems #147111), anti-vGLUT1 guinea pig (Millipore #AB5905), anti-Homer1 rabbit (Synaptic Systems #160003), anti-Parvalbumin rabbit (Swant #PV27a), and anti-SHANK2 guinea pig (Synaptic Systems #162204) and corresponding secondary antibodies. For HALO-Syb2 labeling, slices were incubated overnight at 4 °C with 200 nM HALO ligand JF646 (Promega #GA1120) in PBS. Sections were subsequently washed 3 × 5 mins with PBS, counterstained with DAPI/PBS, and mounted.

Confocal Imaging and Analysis. Images were acquired using a Nikon A1r resonant scanning Eclipse Ti2 HD25 confocal microscope operated by NIS-Elements AR v4.5 acquisition software. Quantification of colocalization using Pearson's correlation coefficient was performed using the colocalization feature of NIS Elements, which automatically measures Pearson's correlation coefficient for a 60× frame. Synaptic puncta were calculated using the Spot Detection feature of NIS Elements. Images were uniformly thresholded in Nikon Elements and Bright Spot Detection used to automatically quantify puncta. For measurements of vGLUT1/Homer1 or vGAT/Gephyrin coclusters, only partially overlapping spots of pre- and postsynaptic markers were counted as coclusters using the Spot Detection feature. MAP2-labeled dendrite lengths were measured to calculate puncta density.

Culture Electrophysiology and Morphology. Voltage-clamp recordings were monitored at RT with a Multiclamp 700B amplifier (Molecular Devices) with cells held at −70 mV. EPSCs or IPSCs were isolated via 50 μM picrotoxin or 50 μM AP5/10 μM CNQX, respectively. Miniature postsynaptic currents were isolated with 1 μM tetrodotoxin. Data were sampled at 10 kHz and analyzed with Clampfit 11.2 (Molecular Devices). For evoked postsynaptic currents (eIPSC and eEPSC), 1 mM QX-314 was added to the internal solution and local stimulation (350 μA) was provided with a concentric bipolar electrode. For biocytin fill, internal solution was made with 2 mg/mL Biocytin and neurons filled with biocytin were labeled with Streptavidin Alexa Fluor 647.

Acute Slice Electrophysiology. Transverse slices (300 μm) were cut by vibratome (Leica VT 1200S) in ice-cold solution containing (in mM) 228 Sucrose, 2.5 KCl, 1 NaH_2PO_4, 26 $NaHCO_3$, 0.5 $CaCl_2$, 7 $MgSO_4$, 11 D-Glucose saturated with 95% O_2/5% CO_2. Slices were transferred to artificial cerebrospinal fluid solution (ACSF) containing (in mM) 119 NaCl, 2.5 KCl, 1 NaH_2PO_4, 26 $NaHCO_3$, 2.5 $CaCl_2$, 1.3 $MgSO_4$, 11 D-Glucose and recovered at 32 °C for 30 min, followed by RT for 1 h. Slices in the recording chamber were continuously perfused with oxygenated ACSF containing 50 μM AP5/10 μM CNQX/1 μM tetrodotoxin to isolate mIPSCs. Whole cell recordings were performed from mClover3 expressing CA1 pyramidal cells while holding at −70 mV.

Data, Materials, and Software Availability. All study data are included in the article and/or *SI Appendix*.

ACKNOWLEDGMENTS. We thank Dr. Colleen Niswender (Vanderbilt University) for kindly sharing mGluR constructs and for advice on mGluR activation. We thank Dr. Thomas C. Südhof (Stanford University) for kindly sharing tagged Lphn mouse lines. We thank Dr. Sylvain Williams (McGill University) for kindly sharing Chrna2-Cre mice. We thank Dr. Stefanie Wieckert (Nikon) for advice on image analysis procedures. We thank Oleg Kovtun (Vanderbilt University) and the Vanderbilt Cell Imaging Shared Resource (CISR) core for advice with Imaris 3D reconstructions. We thank Drs. Ege Kavalali (Vanderbilt University), Vsevolod Gurevich (Vanderbilt University), and all members of the Sando laboratory for critical feedback on the manuscript and study. This study was supported by Grants from the NIH (R00-MH117235 to R.C.S) and Alfred Sloan Foundation (Sloan Fellowship in Neuroscience to R.C.S.).

1. J. R. Sanes, M. Yamagata, Many paths to synaptic specificity. *Annu. Rev. Cell Dev. Biol.* **25**, 161–195 (2009), 10.1146/annurev.cellbio.24.110707.175402.
2. J. R. Sanes, S. L. Zipursky, Synaptic specificity, recognition molecules, and assembly of neural circuits. *Cell* **181**, 536–556 (2020), 10.1016/j.cell.2020.04.008.
3. M. A. Margeta, K. Shen, Molecular mechanisms of synaptic specificity. *Mol. Cell. Neurosci.* **43**, 261–267 (2010), 10.1016/j.mcn.2009.11.009.
4. T. C. Südhof, Towards an understanding of synapse formation. *Neuron* **100**, 276–293 (2018), 10.1016/j.neuron.2018.09.040.
5. T. C. Südhof, The cell biology of synapse formation. *J. Cell Biol.* **220**, e202103052 (2021), 10.1083/jcb.202103052.
6. Z. Nusser, Creating diverse synapses from the same molecules. *Curr. Opin. Neurobiol.* **51**, 8–15 (2018), 10.1016/j.conb.2018.01.001.
7. B. Honig, L. Shapiro, Adhesion protein structure, molecular affinities, and principles of cell-cell recognition. *Cell* **181**, 520–535 (2020), 10.1016/j.cell.2020.04.010.
8. J. de Wit, A. Ghosh, Specification of synaptic connectivity by cell surface interactions. *Nat. Rev. Neurosci.* **17**, 22–35 (2016), 10.1038/nrn.2015.3.

9. T. C. Südhof, Synaptic neurexin complexes: A molecular code for the logic of neural circuits. *Cell* **171**, 745–769 (2017), 10.1016/j.cell.2017.10.024.
10. T. Biederer, M. Stagi, Signaling by synaptogenic molecules. *Curr. Opin. Neurobiol.* **18**, 261–269 (2008), 10.1016/j.conb.2008.07.014.
11. M. B. Dalva, A. C. McClelland, M. S. Kayser, Cell adhesion molecules: Signalling functions at the synapse. *Nat. Rev. Neurosci.* **8**, 206–220 (2007), 10.1038/nrn2075.
12. P. Scheiffele, Cell-cell signaling during synapse formation in the CNS. *Annu. Rev. Neurosci.* **26**, 485–508 (2003), 10.1146/annurev.neuro.26.043002.094940.
13. R. Sando, M. L. Ho, X. Liu, T. C. Südhof, Engineered synaptic tools reveal localized cAMP signaling in synapse assembly. *J. Cell Biol.* **221**, e202109111 (2022), 10.1083/jcb.202109111.
14. H.-B. Kwon, B. L. Sabatini, Glutamate induces de novo growth of functional spines in developing cortex. *Nature* **474**, 100–104 (2011), 10.1038/nature09986.
15. X. Jiang, R. Sando, T. C. Südhof, Multiple signaling pathways are essential for synapse formation induced by synaptic adhesion molecules. *Proc. Natl. Acad. Sci. U.S.A.* **118**, e2000173118 (2021), 10.1073/pnas.2000173118.
16. M. Shahoha, R. Cohen, Y. Ben-Simon, U. Ashery, cAMP-dependent synaptic plasticity at the hippocampal mossy fiber terminal. *Front. Synaptic Neurosci.* **14**, 861215 (2022), 10.3389/fnsyn.2022.861215.
17. A. L. Bauman, A. S. Goehring, J. D. Scott, Orchestration of synaptic plasticity through AKAP signaling complexes. *Neuropharmacology* **46**, 299–310 (2004), 10.1016/j.neuropharm.2003.09.016.
18. M. Mayford, Protein kinase signaling in synaptic plasticity and memory. *Curr. Opin. Neurobiol.* **17**, 313–317 (2007), 10.1016/j.conb.2007.05.001.
19. G. R. Anderson *et al.*, Postsynaptic adhesion GPCR latrophilin-2 mediates target recognition in entorhinal-hippocampal synapse assembly. *J. Cell Biol.* **216**, 3831–3846 (2017), 10.1083/jcb.201703042.
20. D. S. Berns, L. A. DeNardo, D. T. Pederick, L. Luo, Teneurin-3 controls topographic circuit assembly in the hippocampus. *Nature* **554**, 328–333 (2018), 10.1038/nature25463.
21. J. D. Donohue *et al.*, Parahippocampal latrophilin-2 (ADGRL2) expression controls topographical presubiculum to entorhinal cortex circuit connectivity. *Cell Rep.* **37**, 110031 (2021), 10.1016/j.celrep.2021.110031.
22. W. Hong, T. J. Mosca, L. Luo, Teneurins instruct synaptic partner matching in an olfactory map. *Nature* **484**, 201–207 (2012), 10.1038/nature10926.
23. T. J. Mosca, W. Hong, V. S. Dani, V. Favaloro, L. Luo, Trans-synaptic teneurin signalling in neuromuscular synapse organization and target choice. *Nature* **484**, 237–241 (2012), 10.1038/nature10923.
24. M. L. O'Sullivan *et al.*, FLRT proteins are endogenous latrophilin ligands and regulate excitatory synapse development. *Neuron* **73**, 903–910 (2012), 10.1016/j.neuron.2012.01.018.
25. R. Sando, X. Jiang, T. C. Südhof, Latrophilin GPCRs direct synapse specificity by coincident binding of FLRTs and teneurins. *Science* **363**, eaav7969 (2019), 10.1126/science.aav7969.
26. R. Sando, T. C. Südhof, Latrophilin GPCR signaling mediates synapse formation. *eLife* **10**, e65717 (2021), 10.7554/eLife.65717.
27. R. S. Zhang, K. Liakath-Ali, T. C. Südhof, Latrophilin-2 and latrophilin-3 are redundantly essential for parallel-fiber synapse function in cerebellum. *eLife* **9**, e54443 (2020), 10.7554/eLife.54443.
28. X. Zhang, P.-Y. Lin, K. Liakath-Ali, T. C. Südhof, Teneurins assemble into presynaptic nanoclusters that promote synapse formation via postsynaptic non-teneurin ligands. *Nat. Commun.* **13**, 2297 (2022), 10.1038/s41467-022-29751-1.
29. T. Aimi, K. Matsuda, M. Yuzaki, C1ql1-Bai3 signaling is necessary for climbing fiber synapse formation in mature Purkinje cells in coordination with neuronal activity. *Mol. Brain* **16**, 61 (2023), 10.1186/s13041-023-01048-4.
30. J. G. Duman, Y.-K. Tu, K. F. Tolias, Emerging roles of BAI adhesion-GPCRs in synapse development and plasticity. *Neural. Plast.* **2016**, 8301737 (2016), 10.1155/2016/8301737.
31. S. M. Sigoillot *et al.*, The secreted protein C1QL1 and its receptor BAI3 control the synaptic connectivity of excitatory inputs converging on cerebellar Purkinje cells. *Cell Rep.* **10**, 820–832 (2015), 10.1016/j.celrep.2015.01.034.
32. J. R. Stephenson *et al.*, Brain-specific angiogenesis inhibitor-1 signaling, regulation, and enrichment in the postsynaptic density. *J. Biol. Chem.* **288**, 22248–22256 (2013), 10.1074/jbc.M113.489757.
33. J. R. Stephenson, R. H. Purcell, R. A. Hall, The BAI subfamily of adhesion GPCRs: Synaptic regulation and beyond. *Trends Pharmacol. Sci.* **35**, 208–215 (2014), 10.1016/j.tips.2014.02.002.
34. J. Wang *et al.*, RTN4/NoGo-receptor binding to BAI adhesion-GPCRs regulates neuronal development. *Cell* **184**, 5869–5885.e25 (2021), 10.1016/j.cell.2021.10.016.
35. D. Zhu *et al.*, BAI1 regulates spatial learning and synaptic plasticity in the hippocampus. *J. Clin. Invest.* **125**, 1497–1508 (2015), 10.1172/JCI74603.
36. B. D. Ackley, C. elegans fmi-1/flamingo and Wnt pathway components interact genetically to control the anteroposterior neurite growth of the VD GABAergic neurons. *Worm* **2**, e25715 (2013), 10.4161/worm.25715.
37. P.-L. Chen, T. R. Clandinin, The cadherin Flamingo mediates level-dependent interactions that guide photoreceptor target choice in Drosophila. *Neuron* **58**, 26–33 (2008), 10.1016/j.neuron.2008.01.007.
38. R. C. Lee *et al.*, The protocadherin Flamingo is required for axon target selection in the Drosophila visual system. *Nat. Neurosci.* **6**, 557–563 (2003), 10.1038/nn1063.
39. E. M. Mrkusich, D. J. Flanagan, P. M. Whitington, The core planar cell polarity gene prickle interacts with flamingo to promote sensory axon advance in the Drosophila embryo. *Dev. Biol.* **358**, 224–230 (2011), 10.1016/j.ydbio.2011.07.032.
40. E. H. Najarro *et al.*, Caenorhabditis elegans flamingo cadherin fmi-1 regulates GABAergic neuronal development. *J. Neurosci.* **32**, 4196–4211 (2012), 10.1523/JNEUROSCI.3094-11.2012.
41. K.-A. Senti *et al.*, Flamingo regulates R8 axon–axon and axon–target interactions in the Drosophila visual system. *Curr. Biol.* **13**, 828–832 (2003), 10.1016/S0960-9822(03)00291-4.
42. A. Steimel *et al.*, The Flamingo ortholog FMI-1 controls pioneer-dependent navigation of follower axons in C. elegans. *Development* **137**, 3663–3673 (2010), 10.1242/dev.054320.
43. T. Lala, R. A. Hall, Adhesion G protein-coupled receptors: Structure, signaling, physiology, and pathophysiology. *Physiol. Rev.* **102**, 1587–1624 (2022), 10.1152/physrev.00027.2021.
44. T. Langenhan, G. Aust, J. Hamann, Sticky signaling–Adhesion class G protein-coupled receptors take the stage. *Sci. Signal.* **6**, re3 (2013), 10.1126/scisignal.2003825.
45. D. Araç *et al.*, A novel evolutionarily conserved domain of cell-adhesion GPCRs mediates autoproteolysis. *EMBO J.* **31**, 1364–1378 (2012), 10.1038/emboj.2012.26.
46. K. J. Paavola, R. A. Hall, Adhesion G protein-coupled receptors: Signaling, pharmacology, and mechanisms of activation. *Mol. Pharmacol.* **82**, 777–783 (2012), 10.1124/mol.112.080309.
47. A. Vizurraga, R. Adhikari, J. Yeung, M. Yu, G. G. Tall, Mechanisms of adhesion G protein-coupled receptor activation. *J. Biol. Chem.* **295**, 14065–14083 (2020), 10.1074/jbc.REV120.007423.
48. A. N. Dates *et al.*, Heterogeneity of tethered agonist signaling in adhesion G protein-coupled receptors. *Cell Chem. Biol.*, (2024), 10.1016/j.chembiol.2024.03.004.
49. D. L. H. Bui *et al.*, The adhesion GPCRs CELSR1-3 and LPHN3 engage G proteins via distinct activation mechanisms. *Cell Rep.* **42**, 112552. (2023), 10.1016/j.celrep.2023.112552.
50. A. Kishore, R. H. Purcell, Z. Nassiri-Toosi, R. A. Hall, Stalk-dependent and stalk-independent signaling by the adhesion G protein-coupled receptors GPR56 (ADGRG1) and BAI1 (ADGRB1). *J. Biol. Chem.* **291**, 3385–3394 (2016), 10.1074/jbc.M115.689349.
51. S. P. Kordon *et al.*, Structural analysis and conformational dynamics of a holo-adhesion GPCR reveal interplay between extracellular and transmembrane domains. bioRxiv [Preprint] (2024), 10.1101/2024.02.25.581807 (Accessed 27 January 2024).
52. S. Mathiasen *et al.*, G12/13 is activated by acute tethered agonist exposure in the adhesion GPCR ADGRL3. *Nat. Chem. Biol.* **16**, 1343–1350 (2020), 10.1038/s41589-020-0617-7.
53. R. H. J. Olsen *et al.*, TRUPATH, an open-source biosensor platform for interrogating the GPCR transducerome. *Nat. Chem. Biol.* **16**, 841–849 (2020), 10.1038/s41589-020-0535-8.
54. E. Lizano, J. L. Hayes, F. S. Willard, A synthetic method to assay adhesion-family G-protein coupled receptors. Determination of the G-protein coupling profile of ADGRG6(GPR126). *Biochem. Biophys. Res. Commun.* **534**, 317–322 (2021), 10.1016/j.bbrc.2020.11.086.
55. N. A. Perry-Hauser, M. W. VanDyck, K. H. Lee, L. Shi, J. A. Javitch, Disentangling autoproteolytic cleavage from tethered agonist–dependent activation of the adhesion receptor ADGRL3. *J. Biol. Chem.* **298**, 102594 (2022), 10.1016/j.jbc.2022.102594.
56. Y. Wang *et al.*, The GABAB receptor mediates neuroprotection by coupling to G13. *Sci. Signal.* **14**, eaaz4112 (2021), 10.1126/scisignal.aaz4112.
57. D. Matúš, J. M. Lopez, R. C. Sando, T. C. Südhof, Essential role of Latrophilin-1 adhesion GPCR nanoclusters in inhibitory synapses. *J. Neurosci.* **44**, e1978232024 (2023).
58. N. Suzuki, N. Hajicek, T. Kozasa, Regulation and physiological functions of G12/13-mediated signaling pathways. *Neuro-Signals* **17**, 55–70 (2009), 10.1159/000186690.
59. K.-L. Guan, Y. Rao, Signalling mechanisms mediating neuronal responses to guidance cues. *Nat. Rev. Neurosci.* **4**, 941–956 (2003), 10.1038/nrn1254.
60. A. Moers, A. Nürnberg, S. Goebbels, N. Wettschureck, S. Offermanns, Galpha12/Galpha13 deficiency causes localized overmigration of neurons in the developing cerebral and cerebellar cortices. *Mol. Cell. Biol.* **28**, 1480–1488 (2008), 10.1128/MCB.00651-07.
61. D. A. Dettlaff-Swiercz, N. Wettschureck, A. Moers, K. Huber, S. Offermanns, Characteristic defects in neural crest cell-specific Galphaq/Galpha11- and Galpha12/Galpha13-deficient mice. *Dev. Biol.* **282**, 174–182 (2005), 10.1016/j.ydbio.2005.03.006.
62. F. Kobe *et al.*, 5-HT7R/G12 signaling regulates neuronal morphology and function in an age-dependent manner. *J. Neurosci.* **32**, 2915–2930 (2012), 10.1523/JNEUROSCI.2765-11.2012.
63. S. L. Scherer, M. D. Cain, S. M. Kanai, K. M. Kaltenbronn, K. J. Blumer, Regulation of neurite morphogenesis by interaction between R7 regulator of G protein signaling complexes and G protein subunit Gα13. *J. Biol. Chem.* **292**, 9906–9918 (2017), 10.1074/jbc.M116.771923.
64. R. N. Leão *et al.*, OLM interneurons differentially modulate CA3 and entorhinal inputs to hippocampal CA1 neurons. *Nat. Neurosci.* **15**, 1524–1530 (2012), 10.1038/nn.3235.
65. H. Nichol, B. Amilhon, F. Manseau, S. Badrinarayanan, S. Williams, Electrophysiological and morphological characterization of Chrna2 cells in the subiculum and CA1 of the hippocampus: An optogenetic investigation. *Front. Cell. Neurosci.* **12**, 32 (2018), 10.3389/fncel.2018.00032.
66. A. Attardo, J. E. Fitzgerald, M. J. Schnitzer, Impermanence of dendritic spines in live adult CA1 hippocampus. *Nature* **523**, 592–596 (2015), 10.1038/nature14467.
67. E. Alvarez-Curto *et al.*, Targeted elimination of G proteins and arrestins defines their specific contributions to both intensity and duration of G protein-coupled receptor signaling. *J. Biol. Chem.* **291**, 27147–27159 (2016), 10.1074/jbc.M116.754887.
68. M. Grundmann *et al.*, Lack of beta-arrestin signaling in the absence of active G proteins. *Nat. Commun.* **9**, 341 (2018), 10.1038/s41467-017-02661-3.